Stability Analysis of Catenoidal Shaped Liquid Crystalline Polymer Networks

Alejandro D. Rey

Department of Chemical Engineering, McGill University, Montreal, Quebec, Canada H3A 2A7

Received April 18, 1997; Revised Manuscript Received September 15, 1997[⊗]

ABSTRACT: The equations of nematic liquid crystal hydrostatics are used to determine the driving forces that cause the breakup of catenoidal shaped liquid crystalline networks during the phase separation of isotropic and nematic phases. The catenoidal shaped liquid crystalline network is assumed to be an elastic network embedded in an isotropic matrix. The elasticity of the network arises from isotropic surface contributions (interfacial tension) and bulk orientation gradients (Frank elasticity). For liquid crystalline networks with an orientation structure affine to the catenoidal shape, the theory predicts that under certain parametric conditions capillary instabilities will break-up the network by setting up a viscous flow from the thinner sections of the network toward the thicker sections. The stability properties of the liquid crystalline network are summarized in a two-dimensional phase stability diagram, given by the ratio of surface to bulk elasticity as a function of the curvature of the catenoid. Typical parametric conditions for nematic polymers indicate that the liquid crystalline networks are unstable, in qualitative agreement with the findings of Nakai et al. (Nakai, A.; Wang, W.; Hashimoto, T. *Macromolecules* **1996**, *29,* 5288).

1. Introduction

Liquid crystalline materials have been extensively investigated in the past decades[2,3] due to their numerous industrial applications that range, according to molecular weight and mesophase type, from electrooptics[4] to fiber manufacturing.[3,5] Due to the possibility of introducing surface-induced orientation, the interfacial properties of liquid crystals play a predominant role in electrooptical applications.[4,6] For example, physicochemical surface treatments exist which impart a specific molecular orientation at solid−liquid crystal interfaces.[7] Recent developments in the design of multiphase composite materials by thermodynamic instabilities[1] and in liquid crystalline polymer (LCP) fiber manufacturing pose new types of challenging problems involving the stability of liquid crystal fibers and networks and the dynamics of liquid crystalline surfaces. One prominent example arises in the phase separation of thermotropic nematic polymers, in which thermal processing leads to the formation and evolution of various biphasic morphologies involving nematic liquid crystalline and isotropic phases. The presence of internal orientational order, and anisotropic viscoelasticity of the liquid crystalline phase, is a source of additional driving forces in the evolution and coarsening of biphasic systems, as shown by Nakai et al.[1]

A full characterization of the transient morphological phenomena that occur during the phase separation in a polymer admitting isotropic and nematic phases was recently given by Nakai et al.[1] During the thermally-induced phase separation of a thermotropic polyester, a stage designated by Nakai et al.[1] as regime II of the T-jump process is reached. The important morphological feature, identified by Nakai et al.,[1] arising during the phase separation process, is the co-continuous phase morphology of elliptical isotropic droplets traversed by an anisotropic liquid crystalline network, whose channels have a catenoidal shape with a negative Gaussian curvature. Furthermore, they conclude that a quasi-Poiseuille flow within the catenoidal anisotropic channels is set up, driven by capillary pressure. The flow, from the thinnest toward the thickest section of the channels, eventually leads to the network breakdown by a typical pinching process. To generalize the main results of Nakai et al.[1] to other LCP systems, it is necessary to either perform additional experiments with other material systems and at other conditions or to use theory and simulation. In this paper we follow the latter approach.

The main objectives of this paper are as follows: (1) to formulate an anisotropic elastic model that establishes the stability of catenoidal shaped liquid crystalline networks that arise during the phase separation of isotropic and nematic phases; (2) to identify all of the liquid crystalline elastic and capillary contributions to the morphological stability of catenoidal shaped liquid crystalline fibers that arise during the phase separation of isotropic and nematic phases; (3) to present a phase stability diagram for catenoidal shaped nematic networks; (4) to qualitatively compare the model predictions with the experimental data of Nakai et al.[1]

The final breakup morphology, the time scales, the fastest growing modes, and other kinetic effects are not considered in this paper.

The organization of this paper is as follows. In section 2 we define the coordinate system and the state variables and present the governing equations that describe the bulk forces within the network. In section 3 we present and discuss the liquid crystalline network stability analysis. Finally, parameter values arising in the theory are estimated, and the liquid crystalline network stability predictions are calculated and validated with existing experimental data.

2. Governing Equations

2.1. Catenoidal Shaped Nematic Network Microstructure. In this section we establish the mathematical description of the catenoidal shaped nematic liquid crystal network microstructure. A schematic idealized view of a section of the catenoidal shaped liquid crystalline network embedded in an isotropic phase is shown in Figure 1 (left side). The idealized

[⊗] Abstract published in *Advance ACS Abstracts,* November 1, 1997.

S0024-9297(97)00533-0 CCC: $14.00

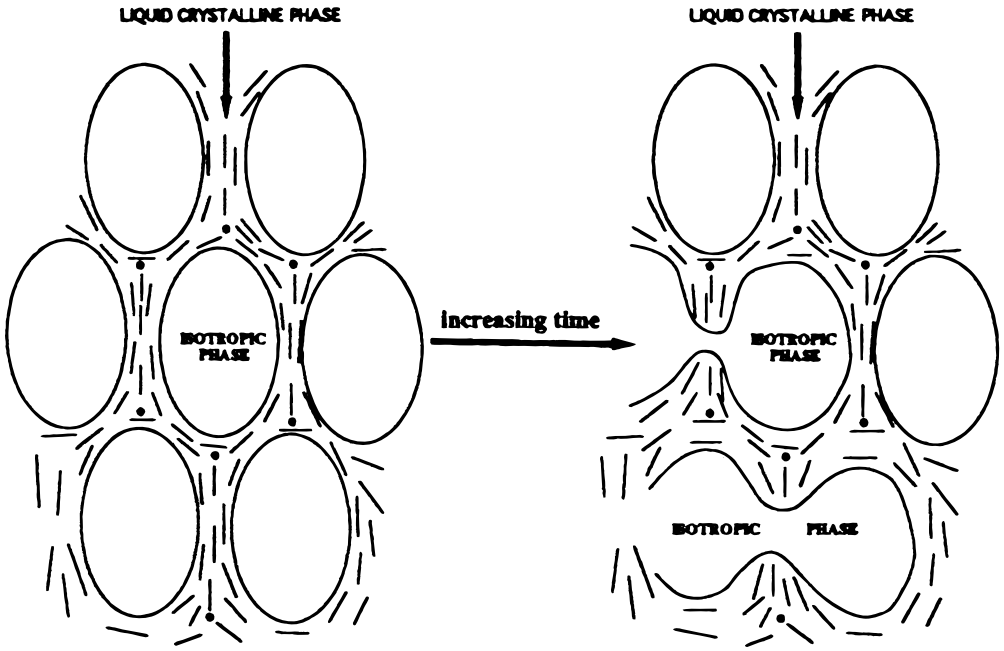

Figure 1. Schematic of a liquid crystalline polymer network traversing an isotropic phase (left), and its breakup (right). The isotropic droplets are elliptical, and the channels containing the liquid crystalline phase are of catenoidal shape. The liquid crystal displays nematic ordering and is affinely oriented with the shape of the channels. The small dots in the liquid crystal phase around the central elliptical droplet (left schematic) denote the $+^1/_2$ edge disclinations. As time increases capillary forces breakup the catenoidal channels (right schematic).

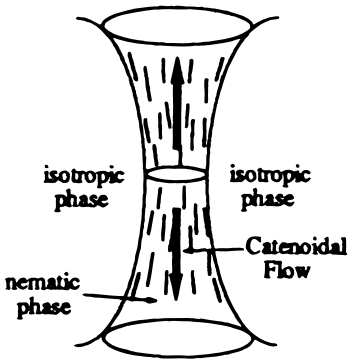

Figure 2. Schematic of the viscous flow that leads to the liquid crystal network breakup. Capillary forces produce a viscous flow (thick arrows) within the catenoidal channels of the liquid crystalline network. The flow is from the thin region toward the thick region and eventually breaks the channel.

morphology is composed of a liquid crystalline network in an isotropic matrix, also known as a percolated network. The section view in Figure 1 shows an isotropic phase of ellipsoidal droplets and a monodomain nematic phase that forms a network. As time progresses, the liquid crystalline network breaks down by pinching in the thinner sections, as indicated on Figure 1 (right side). The essence of the present mathematical analysis is to describe the relevant elastic surfaces and bulk modes in the network that drive the breakup process by a quasi-Poiseuille flow[1] that is generated from the thin sections toward the thicker section of the network, using the well-established equations for the hydrostatics of nematic liquid crystals. An idealized view of a section of the liquid crystal network, showing the observed catenoidal shape[1] and the direction of the viscous flow that eventually leads to the network breakup is shown in Figure 2. In summary, we use a thermodynamic analysis to find out whether a nematic liquid crystal contained in the catenoidal shape and with the orientation shown in Figure 1 (left side) generates a driving force that results in the viscous force depicted by the thick arrows in Figure 2 and thus explain in detail the exact origin of the breakup process shown in Figure 1 (right side).

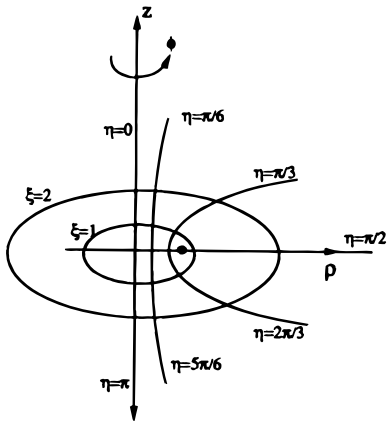

Figure 3. Schematic of the oblate spheroidal coordinate system, used to describe the geometry of the catenoidal channels. The orthogonal coordinates are (ξ, ϕ, η). The catenoidal nematic channels are approximated by hyperboloids of one sheet surfaces, given by the equation $\eta = \eta_o$= c onstant. The dark dot on the $\eta = \pi/2$ axis is the focal point of the hyperbolas. The main surface curvatures at $z = 0$ are functions of η_o.

To best approximate the catenoidal shape shown in Figure 2, we use an oblate spheroidal coordinate system (ξ, η, ϕ), with the z-axis collinear with the axis of the hyperboloid.[8] The coordinate system is shown in Figure 3, and the range of variables is

$$0 \le \xi < \infty; \quad 0 \le \eta \le \pi; \quad 0 \le \phi < 2\pi \quad (1a,b,c)$$

and the relations to the cylindrical (ρ, ϕ, z) coordinates are

$$z = c \sinh \xi \cos \eta; \quad \rho = c \cosh \xi \sin \eta \quad (2a,b)$$

where c is the radius of the focal circle of the confocal family of hyperboloids (noted by a dark circular dot on

Figure 3). Setting $\eta =$ constant generates a hyperboloid of revolution of one sheet, having z as the axis of rotational symmetry. At the thinnest section $z = 0$, and the cross-section normal to the z-axis is a circle of radius $B_o = c \sin \eta_o$. The metric coefficients $[h_\xi, h_\eta, h_\phi]$ for this orthogonal curvilinear coordinate system are

$$h_\xi = h_\eta = \frac{2^{1/2}}{c[\cosh 2\xi + \cos 2\eta]^{1/2}}; \qquad h_\phi = \frac{1}{c \cosh 2\xi \sin 2\eta} \quad (3a,b)$$

To describe the capillary pressure present in the catenoidal channels of the liquid crystal network, we must define the two principal surface curvatures of the hyperboloid of one sheet shown in Figures 2 and 3. For a hyperboloid of one sheet, defined by the equation $\eta = \eta_o =$ constant, the principal surface curvature κ_ξ, κ_ϕ are[9]

$$\kappa_\xi = -h_\eta h_\xi \frac{\partial}{\partial \eta}\left(\frac{1}{h_\xi}\right)\Big|_{\eta=\eta_o} = \frac{2^{1/2}}{c} \frac{\sin 2\eta_o}{(\cosh 2\xi + \cos 2\eta_o)^{3/2}} \quad (4a,b)$$

The average curvature H is then

$$\kappa_\phi = -h_\eta h_\phi \frac{\partial}{\partial \eta}\left(\frac{1}{h_\phi}\right)\Big|_{\eta=\eta_o} = -\frac{2^{1/2}}{c} \frac{\cot \eta_o}{(\cosh 2\xi + \cos 2\eta_o)^{1/2}} \quad (5a,b)$$

$$H = \frac{1}{2}(\kappa_\epsilon + \kappa_\phi) = \frac{2^{1/2}}{2c}\left(\frac{\sin 2\eta_o}{(\cosh 2\xi + \cos 2\eta_o)^{3/2}} - \frac{\cos \eta_o / \sin \eta_o}{(\cosh 2\xi + \cos 2\eta_o)^{1/2}}\right) \quad (6a,b)$$

The director[2] field **n** within the liquid crystal network is assumed to be tangent to the $\eta =$ constant hyperbolas. This implies that as the network forms, the director evolves affinely with the shape of the network. This assumption restricts the director field to

$$\mathbf{n}(\xi,\eta,\phi) = (n_\xi, n_\eta, n_\phi) = (1,0,0) \quad (7)$$

and is shown in Figure 2. Although the director field is constant in this coordinate system, it represents a planar 2-D orientation with splay and bend deformations. Approaching the thinnest region, the elastic deformations vanish since the $\eta =$ constant lines are parallel, but as we move away from this region, the shape of these lines splay and bend, indicating increasing elastic distortions. To provide a justification for the assumed director field, we must consider the orientation conditions at the isotropic−nematic interface. The assumed director field implies that the director has a fixed orientation at the isotropic−nematic interface and that the fixed orientation is tangential to the nematic−isotropic interface and parallel to the axis of the cylindrical symmetry of the catenoid. In the liquid crystal literature the fixed orientation of the director at an interface is known as a strong anchoring condition,[2] while the tangential orientation at the interface is known as planar surface orientation. To establish under which conditions the fixed anchoring condition holds, it is sufficient and necessary to consider the elastic free energy of nematic liquid crystals in a confined (i.e., finite) geometry. The total free energy density F_e of a catenoidal shaped nematic liquid crystal fiber is given by

$$F_e = F_b + F_s \delta(\eta - \eta_o) \quad (8)$$

where F_b is the bulk free energy density, F_s is the surface free energy density, η_o denotes the location of the surface of the catenoidal fiber, and δ is the δ-Dirac functional. The bulk free energy density F_b is given by the sum of the splay, twist, and bend contributions:[2]

$$F_b = F_{splay} + F_{twist} + F_{bend} \quad (9)$$

$$F_{splay} = \frac{K_{11}}{2}(\nabla \mathbf{n})^2; \quad F_{twist} = \frac{K_{22}}{2}(\mathbf{n} \times \nabla \mathbf{n})^2; \qquad F_{bend} = \frac{K_{33}}{2}|(\mathbf{n} \times \text{curl } \mathbf{n})|^2 \quad (10a,b,c)$$

where K_{11}, K_{22}, K_{33} are the temperature dependent Frank elastic constants for splay, twist, and bend, respectively. The surface free energy density F_s is given by the well-known Rapini−Papoular equation:[2]

$$F_s = \gamma + G[1 - (\mathbf{n}\cdot\mathbf{k})^2] \quad (11)$$

where γ is the isotropic interfacial tension (energy/area), G (energy/area) is the orientation dependent contribution to the surface free energy, and **k** is a unit vector that defines the preferred surface orientation, known as the easy axis. In the isotropic phase, at temperatures that exceed the nematic−isotropic transition temperature, G is zero and $F_s = \gamma$, as in isotropic materials. For $G > 0$ the surface energy is a minimum when **n** is parallel to **k**, and in such a case $F_s = \gamma$. In this paper **k** is tangential to the nematic−isotropic interface, defined by $\eta_o =$ constant (see Figure 3). The total free energy F_t of nematic liquid crystalline catenoidal fiber is given by

$$F_t = 2\pi KL \int\int_{\tilde{V}^*} \tilde{F}_b \, d\tilde{V} + 2\pi GDL \int_{\tilde{\Omega}^*} \tilde{F}_s \, d\tilde{\Omega} \quad (12)$$

where $\tilde{F}_b$ is the dimensionless bulk free energy density, $\tilde{F}_s$ is the dimensionless surface free energy density, L is the fiber length, D is the average diameter, K is the average Frank elastic constant (i.e., $K = (K_{11} + K_{22} + K_{33})/3$), $\tilde{V}^*$ is the dimensionless fiber volume, and $\tilde{\Omega}^*$ is the dimensionless fiber lateral surface area. From eq 12 it follows that the ratio of the characteristic bulk free energy to the characteristic surface free energy is equal to $K/(DG)$. If $K/(DG)$ is of order much less than 1, the bulk free energy is insignificant when compared to the surface free energy, and energy minimization in the catenoidal geometry is achieved by a nonhomogeneous bulk director field but with a fixed surface director orientation parallel to the easy axis **k**. Thus, the assumption of a fixed surface director orientation is applicable if $K/(DG)$ is sufficiently small. If $K/(DG)$ is of order 1, the surface director deviates from the easy axis (i.e., $\mathbf{n} \neq \nu$), and the contribution of the term introduced by G in eq 11 must be included in the analysis. In this paper we assume that $K/(DG) \ll 1$. Using typical values[2−4] ($K = 10^{-7}$ erg/cm, $G = 1$ erg/cm^{-2}, $D = 10^{-4}$ cm), we find $K/(DG) = 10^{-3}$.

In summary, the already justified (see above) assumptions, the realistic parametric restrictions imposed

on the analysis, and the selected model geometry are as follows:

(1) The relevant structural unit of the liquid crystalline network is approximated by a hyperboloid of one sheet (Figures 1−3).

(2) The main structural features of the network are described by the director field of a uniaxial nematic liquid crystal.

(3) The director field within the hyperboloid is a constant in an oblate spheroidal coordinate system.

(4) The director surface orientation is always tangential to the isotropic−nematic interface, and the surface free energy density is isotropic since the surface director orientation is along the easy axis.

Situations involving microstructure or geometry not restricted as above lie beyond the range of validity of the present analysis, and beyond the scope of this paper.

2.2. Hydrostatic Equations. According to the hydrostatic principles for nematic liquid crystals, the bulk force Φ generated by a pressure field and free energy distortions in a nematic liquid crystal is given by[2]

$$\Phi = -\nabla(F_e + p) \tag{13}$$

where ∇ is the gradient operator, F_e is the total Frank elastic energy density, and p is the pressure field. At the surface of the hyperboloid the pressure is given by the Young−Laplace equation:[9]

$$p|_{\eta_o} = p_+|_{\eta_o} - p_-|_{\eta_o}; \quad p_+ = \gamma\kappa_\phi; \quad p_- = -\gamma\kappa_\xi \tag{14a,b,c}$$

The condition that leads to a positive force and to the network breakup depends on the combined effects of Frank elasticity and interfacial tension,

$$\Phi|_{\eta_o} = -\frac{\partial}{\partial\xi}(F_e + 2H\gamma)|_{\eta_o} > 0 \tag{15}$$

This positive force drives the viscous flow from the thinnest section of the hyperboloid toward the thicker section of the hyperboloid, as shown by the thick vertical arrows in Figure 2. The network breakup is thus an elastic instability that contains surface (interfacial tension) and bulk (Frank elasticity) contributions.

3. Stability Analysis of Catenoidal Shaped Liquid Crystal Networks

As identified by Nakai et al.,[1] the breakup is due to the viscous flow from thinner to thicker parts of the network, and as shown in this paper, the viscous flow arises from a reduction of bulk Frank elastic and interfacial energy.

Replacing the director field in the Frank energy, we find that the scaled splay contribution S is

$$S|_{\eta_o} = \frac{F_S c^2}{K_{11}}|_{\eta_o} = \frac{1}{(\cosh 2\xi + \cos 2\eta_o)} \times \left[\frac{\sinh 2\xi}{\cosh 2\xi + \cos 2\eta_o} + \frac{\sinh \xi}{\cosh \xi}\right]^2 \tag{16}$$

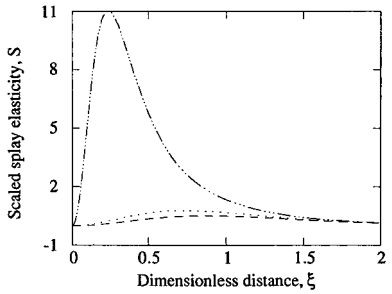

Figure 4. Scaled splay contribution $S(F_S c^2/K_{11})$ as a function of distance ξ for three values of η_o: $\pi/20$ (dashed line); $\pi/10$ (dotted line); $\pi/5$ (dashed−dotted line). For any η_o the splay energy profile has a local maximum, which increases in magnitude with increasing η_o. For ξ close to zero splay modes stabilize the network.

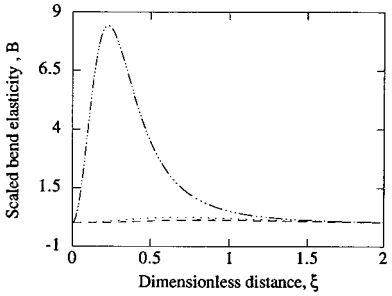

Figure 5. Scaled bend contribution $B(F_B c^2/K_{33})$ as a function of distance ξ for three values of η_o: $\pi/20$ (dashed line); $\pi/10$ (dotted line); $\pi/5$ (dashed−dotted line). For any η_o the bend energy profile has a local maximum, which increases in magnitude with increasing η_o. Thus, in the vicinity of the thinnest network section (i.e., for ξ close to zero) bend modes stabilize the network, since the energy profile $\partial B/\partial\xi$ has a positive slope.

and that the scaled bend contribution B is

$$B|_{\eta_o} = \left.\frac{F_B c^2}{K_{33}}\right|_{\eta_o} = \frac{1}{(\cosh 2\xi + \cos 2\eta_o)} \times \left[\frac{\sin 2\eta_o}{(\cosh 2\xi + \cos 2\eta_o)}\right]^2 \tag{17}$$

Figure 4 shows the scaled splay contribution S as a function of distance ξ for three values of η_o: $\pi/20$ (dashed line); $\pi/10$ (dotted line); $\pi/5$ (dashed−dotted line). For any η_o the splay energy profile has a local maximum, which increases in magnitude with increasing η_o. Thus, in the vicinity of the thinnest network section (i.e., for ξ close to zero) splay modes stabilize the network, since the energy profile $\partial S/\partial\xi$ has a positive slope. Figure 5 shows the scaled bend contribution B as a function of distance ξ for the three values of η_o used in Figure 4. For any η_o the bend energy profile has a local maximum, which increases in magnitude with increasing η_o. Thus, in the vicinity of the thinnest network section (i.e., for ξ close to zero) bend modes stabilize the network, since the energy profile $\partial B/\partial\xi$ has a positive slope. Therefore, Frank elasticity stabilizes the network.

Replacing the director field in the Laplace−Young equation, we find that the scaled positive pressure contribution P_+ arising from κ_ϕ is

$$P_+|_{\eta_o} = \left.\frac{p_+ c}{2^{1/2}\gamma}\right|_{\eta_o} = \frac{\cos \eta_o}{\sin \eta_o[\cosh 2\xi + \cos 2\eta_o]^{1/2}} \tag{18}$$

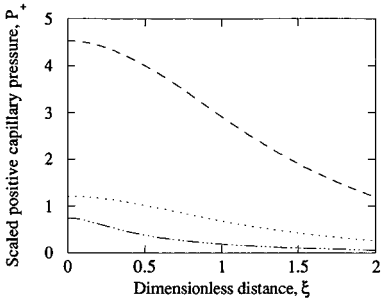

Figure 6. Scaled positive capillary pressure contribution P_+ (see eq 18) as a function of distance ξ for three values of η_o: $\pi/20$ (dashed line); $\pi/10$ (dotted line); $\pi/5$ (dashed−dotted line). For any η_o the positive capillary pressure is a monotonically decreasing function of ξ, which decreases in magnitude with increasing η_o. The positive capillary pressure P_+ destabilizes the network, since the energy profile $\partial P_+/\partial\xi$ has a negative slope.

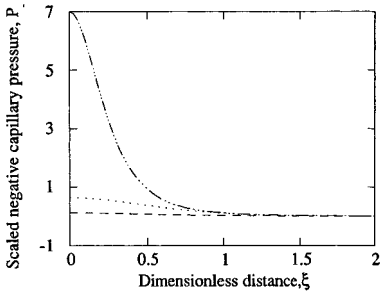

Figure 7. Scaled negative capillary pressure contribution P_- (see eq 19) as a function of distance ξ for three values of η_o: $\pi/20$ (dashed line); $\pi/10$ (dotted line); $\pi/5$ (dashed−dotted line). For any η_o the negative capillary pressure is a monotonically decreasing function of ξ, which increases in magnitude with increasing η_o. The negative capillary pressure stabilizes the network, since the energy profile $-\partial P_-/\partial\xi$ has a positive slope. Therefore the curvature κ_ϕ is the driving force for the network breakdown.

and that the scaled negative capillary pressure contribution P_- arising from κ_ξ is

$$P_-|_{\eta_o} = \frac{p_- c}{2^{1/2}\gamma}|_{\eta_o} = \frac{\sin 2\eta_o}{(\cosh 2\xi + \cos 2\eta_o)^{3/2}} \qquad (19)$$

Figure 6 shows the scaled positive capillary pressure contribution P_+ as a function of distance ξ for the three values of η_o used in Figure 4. For any η_o the positive capillary pressure is a monotonically decreasing function of ξ, which decreases in magnitude with increasing η_o. Thus, in the vicinity of the thinnest network section (i.e., for ξ close to zero) the positive capillary pressure destabilizes the network, since the energy profile $\partial P_+/\partial\xi$ has a negative slope. Figure 7 shows the scaled negative capillary pressure contribution P_- as a function of distance ξ for the three values of η_o used in Figure 4. For any η_o the negative capillary pressure is a monotonically decreasing function of ξ, which increases in magnitude with increasing η_o. To find the nature of the negative capillary pressure effect on the stability of the network, we recall that the total capillary pressure is given by $P = P_+ - P_-$. Thus, in the vicinity of the thinnest network section (i.e., for ξ close to zero) the negative capillary pressure stabilizes the network, since the energy profile $-\partial P_-/\partial\xi$ has a positive slope. Therefore, the curvature κ_ϕ is the driving force for the network breakdown.

Having identified the stabilizing and destabilizing elastic forces, we next construct the stability phase

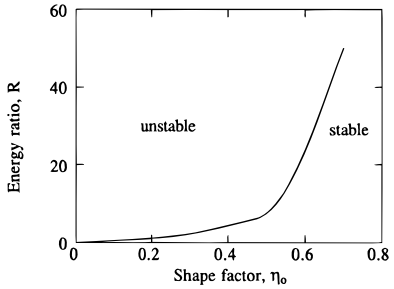

Figure 8. Stability diagram for a liquid crystalline network, presented in the parametric plane spanned by the ratio of surface to bulk energy ($R = 2^{/12}\gamma c/K$) and by the shape factor η_o. For $\eta_o > 0$ the network is stable for any R. The reason is that at $\eta_o = \pi/4$ the average curvature is zero, $H = 0$, and for $\eta_o > \pi/4$ the negative pressure will stabilize the network. Thinner fiberlike hyperboloids become unstable at lower values of R, while thicker hyperboloids become unstable at higher values of R.

diagram for a liquid crystalline network. Without loss of the essential nature of the mechanism that governs the stability of catenoidal liquid crystalline networks, we assume that the splay elastic constant is equal to the bend elastic constant: $K_{11} = K_{33} = K$. This is a frequently used approximation[2] by workers in the field since it greatly simplifies the mathematics at some cost in accuracy. To assess the accuracy loss when using the equal splay−bend constant approximation, we can compute the normalized elastic anisotropy Δ

$$\Delta = \frac{2|K_{11} - K_{33}|}{K_{11} + K_{33}} \qquad (20)$$

of well-characterized LCPs. For the lyotropic nematic liquid crystal polymer PBG,[10] we find $\Delta = 0.068$. It is important to note that in the present case the equal splay−bend approximation is a useful simplifying assumption because the network's stability is not governed by the balance between splay and bend distortions; in other words, it is not driven by the magnitude of Δ. The only two parameters that determine the network stability are the shape factor η_o and the characteristic elastic energy ratio R of interfacial tension to Frank bulk elasticity. Thus, the net impact of the equal splay−bend approximation is on the exact location of the stability envelope, that is, the threshold values of the shape parameter and elasticity ratio R at which the catenoidal shape becomes unstable. The expression for energy ratio R, found by dividing the potential $(F_e + p)$ with K/c^2, is given by

$$R = 2^{1/2}\gamma c/K \qquad (21)$$

To construct the stability diagram, we check the sign of the slope of the scaled potential $(F_e + p)c^2/K$ at the origin $\xi = 0$: if the slope is positive (negative), the network is stable (unstable). Figure 8 shows the stability diagram for a liquid crystalline network, presented in the parametric plane spanned by the ratio of surface to bulk energy and by the shape factor η_o. The figure shows that for $\eta_o > 0$ the network is stable for any R. The reason is that at $\eta_0 = \pi/4$ the average curvature is zero, $H = 0$, and for $\eta_o > \pi/4$ the negative pressure will stabilize the network. The figure shows the parametric values for stability and instability. Thinner fiberlike hyperboloids become unstable at lower values of R, while thicker hyperboloids become unstable at higher values of R.

For typical material parameters[11,12] we may use $K = 10^{-7}$erg/cm, $\gamma = 1$ erg/cm^2, and $c = 1$ μm, which gives an energy ratio of $R = 10^3$. For a typical hyperboloid with $\eta_o = \pi/5$ or less Figure 8 shows that the network is unstable. This is in qualitative agreement with the findings of Nakai et al.[1]

4. Conclusions

The equations of nematic liquid crystal hydrostatics are used to characterize the breakup of a liquid crystalline anisotropic network. The network elasticity contains isotropic surface contributions and anisotropic bulk elastic modes. For liquid crystalline networks with an internal orientation pattern affine to the shape of the network, the model predicts that under certain parametric conditions capillary forces will induce a viscous flow from thinner to thicker regions and eventually lead to the network breakup. The parametric conditions that promote the network breakup are high interfacial tension, low Frank elasticity, and thin catenoidal channels. The stability phase diagram for liquid crystalline networks is a two-dimensional plot that identifies parametric conditions that lead to stable and unstable networks; it is constructed from the parametric dependence of the bulk driving force that breaks-up the network on the shape of the network and on the ratio of surface to bulk elasticity. Using typical values for nematic polymers, it is found that the liquid crystalline network will breakdown, in qualitative agreement with the findings of Nakai et al.[1]

Acknowledgment. This work is supported by a grant from the Natural Sciences and Engineering Research Council of Canada.

References and Notes

(1) Nakai, A.; Wang, W.; Hashimoto, T. *Macromolecules* **1996**, *29*, 5288.
(2) de Gennes, P. G.; Prost, J. *The Physics of Liquid Crystals*, 2nd ed.; Oxford University Press: London, 1993.
(3) Donald, A. M.; Windle, A. H. *Liquid Crystalline Polymers*; Cambridge University Press: Cambridge, U.K., 1992.
(4) Blinov, L. M.; Chigrinov, V. G. *Electrooptic Effects in Liquid Crystal Materials*; Springer-Verlag: New York, 1994.
(5) Srinivasarao, M. *Int. J. Mod. Phys. B* **1995**, *18/19*, 2515.
(6) Sonin, A. A. *The Surface Physics of Liquid Crystals*; Gordon and Breach Publishers: New York, 1995.
(7) Goossens, W. J. A. *Mol. Cryst. Liq. Cryst.* **1985**, *124*, 305.
(8) Happel, J.; Brenner, H. *Low Reynolds Number Hydrodynamics*; Martinus Nijhoff Publishers: Dordrecht, The Netherlands, 1983.
(9) Edwards, D. A.; Brenner, H.; Wasan, D. T. *Interfacial Transport Processes and Rheology*; Butterworth-Heinemann: Stoneham, 1991.
(10) Taratuta, V. G.; Hurd, A. J.; Meyer, R. B. *Phys. Rev. Lett.* **1985**, *55*, 246.
(11) Se, K.; Berry, G. *Mol. Cryst. Liq. Cryst.* **1987**, *153*, 133.
(12) Doi, M.; Kuzuu, N. *J. Appl. Polym. Sci.: Appl. Polym. Symp.* **1985**, *41*, 65.

MA9705331